JOURNAL OF VIROLOGY, July 2008, p. 6984–6991 Vol. 82, No. 14
0022-538X/08/$08.00+0 doi:10.1128/JVI.00442-08

Structural Analysis of Major Species Barriers between Humans and Palm Civets for Severe Acute Respiratory Syndrome Coronavirus Infections[▽]

Fang Li*

University of Minnesota, Minneapolis, Minnesota 55455

Received 28 February 2008/Accepted 21 April 2008

It is believed that a novel coronavirus, severe acute respiratory syndrome coronavirus (SARS-CoV), was passed from palm civets to humans and caused the epidemic of SARS in 2002 to 2003. The major species barriers between humans and civets for SARS-CoV infections are the specific interactions between a defined receptor-binding domain (RBD) on a viral spike protein and its host receptor, angiotensin-converting enzyme 2 (ACE2). In this study a chimeric ACE2 bearing the critical N-terminal helix from civet and the remaining peptidase domain from human was constructed, and it was shown that this construct has the same receptor activity as civet ACE2. In addition, crystal structures of the chimeric ACE2 complexed with RBDs from various human and civet SARS-CoV strains were determined. These structures, combined with a previously determined structure of human ACE2 complexed with the RBD from a human SARS-CoV strain, have revealed a structural basis for understanding the major species barriers between humans and civets for SARS-CoV infections. They show that the major species barriers are determined by interactions between four ACE2 residues (residues 31, 35, 38, and 353) and two RBD residues (residues 479 and 487), that early civet SARS-CoV isolates were prevented from infecting human cells due to imbalanced salt bridges at the hydrophobic virus/receptor interface, and that SARS-CoV has evolved to gain sustained infectivity for human cells by eliminating unfavorable free charges at the interface through stepwise mutations at positions 479 and 487. These results enhance our understanding of host adaptations and cross-species infections of SARS-CoV and other emerging animal viruses.

Emerging animal viruses impose major threats to human health. Knowledge about how they adapt to different hosts and how they cross species barriers between hosts is important for preventing and curtailing infectious viral diseases. A novel coronavirus, severe acute respiratory syndrome coronavirus (SARS-CoV), is the agent of SARS (7, 18, 23, 25). SARS-CoV first emerged in Guangdong, China, in 2002 to 2003. Within several months it caused over 8,000 infections worldwide, with a fatality rate of ~10% (9, 32). It reemerged in Guangdong in 2003 to 2004, with four sporadic infections, no fatalities, and no subsequent human-to-human transmission (5, 16, 27). SARS has been absent in humans ever since. During the SARS outbreak, palm civets and raccoon dogs in Guangdong animal markets harbored viruses highly similar to human viral strains (5). In 2005 to 2006 the virus was found again in civets (17). It is believed that civets passed the virus to humans and caused the SARS epidemic (14, 26). This study investigates the barriers of the cross-species infections by the virus and the structural basis for viral evolution that overcame the barriers to allow the virus to infect humans.

Several lines of evidence suggest that civets served as the direct source of SARS-CoV that infected humans in both 2002 to 2003 and 2003 to 2004. During the epidemic, SARS-CoV was isolated from most marketplace civets (5). It persisted in civets for weeks (30). In addition, all SARS patients in 2003 to 2004 had a history of close contact with civets (16, 27). Culling of civets may be responsible for the absence of SARS-CoV in humans since 2003 to 2004 (33). Critically, biochemical and structural studies of virus-receptor interactions reveal close evolutionary relationships among the civet and human viral strains and thus support the critical roles of civets in transmitting SARS-CoV to humans, as discussed below.

The major species barriers between humans and civets for SARS-CoV infections are the specific interactions between the virus and its host receptor. SARS-CoV uses a cell surface zinc peptidase, angiotensin-converting enzyme 2 (ACE2), as its receptor (13). A previous study showed that human ACE2 contains a claw-like N-terminal peptidase domain, with two lobes harboring the active site in a deep groove (28). SARS-CoV enters cells through the activities of a spike protein on its envelope. The spike protein has a receptor-binding region (S1) and a membrane fusion region (S2) (8). During cell entry, a defined receptor-binding domain (RBD) on S1 binds ACE2, resulting in viral attachment (1, 29, 31); subsequently, S2 fuses viral and host membranes. Which host is susceptible to SARS-CoV is primarily determined by the affinity between the virus and host ACE2 in the initial viral attachment step. Increasing the binding affinity between RBD and ACE2, either by changing one or a few residues at their interface or by expressing variants of the proteins in transgenic animals, can transform a previously ineffective host to an effective one (12, 15, 19, 20, 24). For example, there are four prototypic SARS-CoV strains: hTor02 (a human strain isolated in 2002 to 2003), cSz02 (a

* Mailing address: Department of Pharmacology, University of Minnesota Medical School, 6-121 Jackson Hall, 321 Church St. S.E., Minneapolis, MN 55455. Phone: (612) 625-6149. Fax: (612) 625-8408. E-mail: lifang@umn.edu.

▽ Published ahead of print on 30 April 2008.

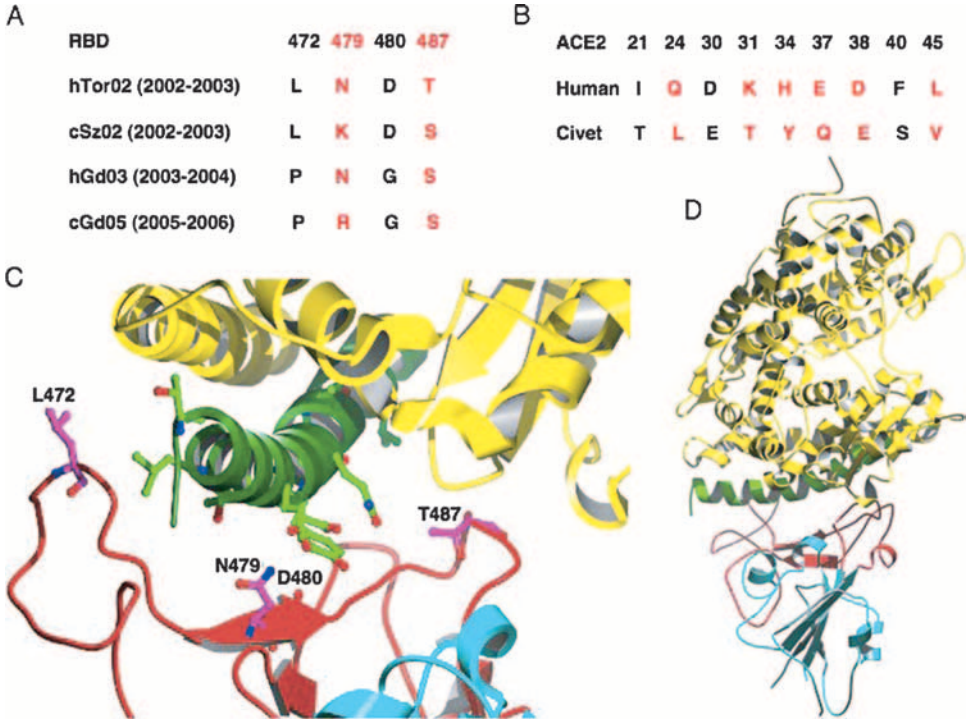

FIG. 1. The SARS-CoV/receptor interface. (A) Alignment of residues on the SARS-CoV RBD at the interface that have undergone evolution. In red are two residues, residues 479 and 487, that determine the major species barriers between human and civet for SARS-CoV infections. Four prototypic viral strains are defined in the text. (B) Alignment of residues on the N-terminal helix of ACE2 that differ between human and civet. In red are residues that directly interact with SARS-CoV. (C) Crystal structure of the interface between hTor02 RBD and chimeric ACE2 bearing the N-terminal helix from civet and the remaining peptidase domain from human. The receptor-binding motif (RBM) on hTor02 RBD is in red, with side chains of the four residues that have undergone evolution (residues 472, 479, 480, and 487). The N-terminal helix from civet ACE2 is in green, with side chains of residues that differ between human and civet. The rest of peptidase domain from human ACE2 is in yellow. (D) An overall view of the crystal structure of human-civet chimeric ACE2 complexed with hTor02 RBD. The structure is rotated clockwise in depth compared with the structure in panel C. The illustrations were made using Povscript (4).

civet strain isolated in 2002 to 2003), hGd03 (a human strain isolated in 2003 to 2004), and cGd05 (a civet strain isolated in 2005 to 2006) (Fig. 1A) (5, 17, 27). Human ACE2 has high affinity for hTor02 RBD, moderate affinity for hGd03 RBD, and poor affinities for cSz02 and cGd05 RBDs. In contrast, civet ACE2 has high affinities for all of the four RBDs (15, 17). Correspondingly, humans are most susceptible to hTor02, while civets are susceptible to all four viral strains (15, 17).

Biochemical and structural studies have further pinpointed mutations on SARS-CoV RBD that are critical for the civet-to-human transmission of the virus. A previously determined crystal structure of human ACE2 complexed with the hTor02 RBD shows that RBD presents a gently concave surface cradling the outer surface of the N-terminal lobe of the ACE2 peptidase domain (11). Four RBD residues at the interface differ in human and civet viral isolates and may potentially be critical for the cross-species infections with SARS-CoV (Fig. 1A). Two of these RBD residues, residues 472 and 480, have little effect on receptor binding or viral infectivity and thus are excluded as major factors in receptor binding and viral infections (15, 24). The other two of these RBD residues at the interface, residues 479 and 487, have remarkable effects on receptor binding and viral infectivity. Residue 479 is an asparagine in most human viral isolates but can be asparagine, lysine, or arginine in civet viral isolates. Residue 487 is a threonine in all human viral isolates from the 2002 to 2003 epidemic but is a serine in human viral isolates from the mild 2003 to 2004 infections as well as in all civet viral isolates. The N479K and T487S single mutations on hTor02 RBD decrease the protein's binding affinity for human ACE2 by over 30- and 20-fold, respectively (15). The N479K/T487S double mutation on hTor02 RBD decreases both the protein's binding affinity for human ACE2 and viral infectivity for human cells by over 1,000-fold (15, 24). Conversely, the K479N and S487T mutations on cSz02 RBD dramatically increase the protein's binding affinity for human ACE2 and viral infectivity for human cells (15, 24). Curiously, neither the N479K nor the T487S mutation on hTor02 RBD has dramatic effects on the protein's binding affinity for civet ACE2 or viral infectivity for civet ACE2-expressing cells (15, 24). Overall, these results suggest that human ACE2, but not civet ACE2, is extremely sensitive to mutations at positions 479 and 487 in viral RBD. What is the structural basis for each of these mutations on SARS-CoV RBD? What factors determine the different receptor activities of human and civet ACE2s? What are the epidemic implications of these viral mutations and receptor activities? These questions cannot be satisfactorily answered based on one crystal structure. To address these questions, in the current study three more crystal structures have been determined, detailing interactions between civet ACE2 and viral strains hTor02,

TABLE 1. Crystallographic data collection and refinement statistics

Category and parameter	Value for complex of chimeric ACE2 and RBD from:		
	hTor02	cSz02	cGd05
Data[a]			
Space group	$P2_1$	$P2_1$	$P2_1$
Cell constants (Å, °)	a = 80.0, b = 119.8, c = 108.8, β = 96.2	a = 80.4, b = 119.8, c = 109.4, β = 95.9	a = 80.4, b = 119.8, c = 109.8, β = 95.5
Resolution (Å)	50 − 2.8	50 − 3.1	50 − 2.9
Mosaicity (°)	0.6	0.5	0.7
R_{symm} (last shell) (%)[b]	6.2 (37.3)	14.4 (84.7)	7.9 (83.2)
Observed reflections	758,569	485,595	768,112
Unique reflections	50,660	38,826	46,550
Completeness (last shell) (%)	95.0 (64.1)	98.9 (94.7)	99.5 (99.8)
I/σ (last shell)	19.1 (2.3)	11.4 (1.3)	19.0 (1.8)
Refinement			
R_{work} (R_{free}) (%)[c]	21.4 (27.9)	22.0 (30.2)	22.4 (27.9)
R_{free} reflections (%)	5	5	5
Correlation coefficient ($F_0 - F_c$)	0.934	0.920	0.930
Correlation coefficient ($F_0 - F_c$) (free)	0.894	0.857	0.892
Bond lengths (Å) root mean square	0.010	0.011	0.010
Bond angles (°) root mean square	1.270	1.293	1.243
CHIRAL root mean square	0.090	0.084	0.082

[a] Data were collected at λ = 0.979 Å at APS beamline 19BM.
[b] $R_{symm} = \Sigma_{i,h} I_{i,h} - \langle I_h \rangle / \Sigma_{i,h} I_{i,h}$, where $\langle I_h \rangle$ is the mean of the i observations of the reflection h.
[c] $R_{work} = \Sigma \| F_0 - F_c \| / \Sigma F_0$. R_{free} is the same statistic but is calculated from a subset of the data (5%) that has not been used using refinement.

cSz02, and cGd05. Taken together, these structures have revealed some of the major species barriers between humans and civets for SARS-CoV infections and the viral evolution that overcame the barriers.

MATERIALS AND METHODS

Protein purification and crystallization. The chimeric ACE2 was constructed by mutating residues on the N-terminal helix of human ACE2 to their corresponding residues on civet ACE2. The cSz02 and cGd05 RBDs were constructed by mutating residues 479, 480, and 487 on hTor02 RBD to their corresponding residues on cSz02 and cGd05 RBDs. All the mutations were made by site-directed mutagenesis. The human, civet, and chimeric ACE2s and hTor02, cSz02, and cGd05 RBDs were each expressed and purified as previously described (11). To purify the complex of the chimeric ACE2 and each of the three RBDs, the chimeric ACE2 was incubated with excess RBD for 30 min at room temperature in buffer A (20 mM Tris [pH 7.5], 150 mM NaCl). The mixture was then purified on a Superdex 200 gel filtration column (GE Healthcare) in buffer A. Fractions containing the complex were pooled and concentrated to 10 mg/ml with Centriprep (Amicon). The same protocol was also used for solution RBD binding assays with human, civet, and chimeric ACE2s.

Crystals were grown in sitting drops at room temperature, over wells containing 100 mM Tris (pH 8.5), 22% polyethylene glycol 6000, and 100 mM NaCl. The drops were made by mixing 5 μl complex in buffer A with 5 μl well solution. Crystals first appeared in 2 days and were allowed to grow for another 7 days before being harvested. Harvested crystals were soaked briefly in 100 mM Tris (pH 8.2), 30% polyethylene glycol 6000, 150 mM NaCl, and 30% ethylene glycol and flash frozen in liquid nitrogen.

Structure determination and refinement. X-ray diffraction data were collected at Argonne Photon Source (Argonne, IL) beamline 19BM and processed using HKL2000 (22). Using program CNS (2), each structure was determined by molecular replacement using the structure of human ACE2 complexed with hTor02 RBD as the search model (accession number 2AJF). Each of the crystals contains two complexes per asymmetric unit. Electron densities were improved by noncrystallographic symmetry averaging of the two copies of the complexes using CCP4 DM (3). Residue changes of the models were done using program O (6). The structures were refined using programs CNS (2) and CCP4 refmac (21). Data and refinement statistics are shown in Table 1.

Protein structure accession numbers. Coordinates and structure factors have been submitted to the Protein Data Bank under accession numbers 3D0G (complex of chimeric ACE2 and hTor02 RBD), 3D0H (complex of chimeric ACE2 and cSz02 RBD), and 3D0I (complex of chimeric ACE2 and cGd05 RBD).

RESULTS

Construction of a human-civet chimeric ACE2. To study the interactions between civet ACE2 and RBDs, this study constructed a human-civet chimeric ACE2 bearing the N-terminal helix from civet and the remaining peptidase domain from human (Fig. 1B). The N-terminal helix of ACE2 sits on top of the base of the concave surface presented by RBD and mediates most of the interactions with RBD (11, 15) (Fig. 1C and D). The ACE2-binding region on RBD is rich in tyrosine and forms a tight hydrophobic sheath surrounding the N-terminal helix of ACE2 (11). Importantly, compared to the remainder of the ACE2 sequence, the N-terminal helix is among the more divergent areas among mammals. Thus, adaptations of the virus to the N-terminal helix of host ACE2 are critical for viral infections. cSz02 and cGd05 RBDs were also constructed in this study by mutating residues 479, 480, and 487 on hTor02 RBD to the corresponding residues on cSz02 and cGd05 RBDs. Each of the three ACE2 (human, civet, and chimeric) and the three RBDs (hTor02, cSz02, and cGd05) was expressed and purified as previously described (11).

The receptor activity of the chimeric ACE2 is assayed by its binding affinity for different RBDs in solution. To do the binding assays, one of the three RBDs (hTor02, cSz02, or cGd05) is incubated with one of the three ACE2s (human, civets or chimeric) in solution with the RBD in excess, and then different components of the mixture are separated on a gel filtration chromatography column. The elution volume of the RBD/ACE2 complex is smaller than that of the ACE2, and thus RBD binding leads to leftward shift of the ACE2-containg peak. A complete shift suggests tight binding between ACE2

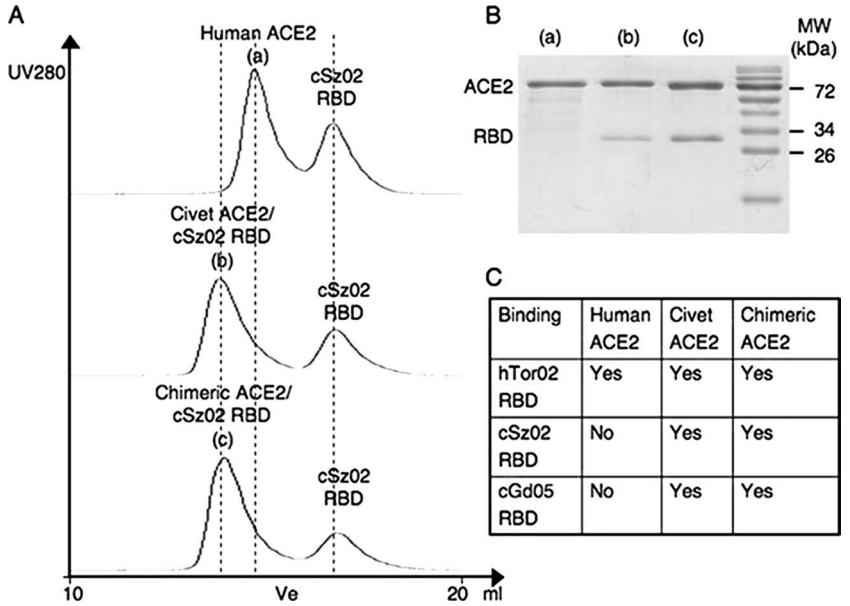

Binding	Human ACE2	Civet ACE2	Chimeric ACE2
hTor02 RBD	Yes	Yes	Yes
cSz02 RBD	No	Yes	Yes
cGd05 RBD	No	Yes	Yes

FIG. 2. Solution RBD binding assays of human, civet, and chimeric ACE2. (A) Gel filtration chromatography on Superdex 200 of a mixture of human ACE2 and cSz02 RBD (top), a mixture of civet ACE2 and cSz02 RBD (middle), and a mixture of chimeric ACE2 and cSz02 RBD (bottom). The cSz02 RBD is in excess in each of the three mixtures. The dotted lines mark the relative elution volumes of the proteins. A leftward shift indicates binding. Peak a corresponds to unbound human ACE2. Peaks b and c correspond to cSz02 RBD-bound civet ACE2 and chimeric ACE2, respectively. (B) Reducing sodium dodecyl sulfate-polyacrylamide gel electrophoresis and Coomassie blue staining of peaks a, b, and c in panel A, confirming the protein components of each of the three peaks. The bands corresponding to RBD and ACE2 were confirmed by protein N-terminal sequencing (10). (C) Summary of receptor activities of human ACE2, civet ACE2, and chimeric ACE2. The latter two have the same receptor activity, which is different from that of human ACE2.

and RBD, a partial shift suggests moderate binding, and no shift suggests weak or no binding (Fig. 2A). The protein components of the peaks are further confirmed by reducing sodium dodecyl sulfate-polyacrylamide gel electrophoresis and Coomassie blue staining (Fig. 2B). The results show that both the chimeric ACE2 and civet ACE2 bind cSz02 and cGd05 RBDs with high affinities in solution, whereas human ACE2 binds cSz02 and cGd05 RBDs poorly (Fig. 2C). Therefore, the chimeric ACE2 has the same receptor activity as civet ACE2. The chimeric ACE2 was chosen for structural studies over civet ACE2, because the former, and not the latter, yields good-quality crystals when complexed with RBD.

Structure determination and overall structure. Because of the tight binding between chimeric ACE2 and each of the three RBDs (hTor02, cSz02, and cGd05), each of the three complexes was purified by gel filtration chromatography and subsequently crystallized in the same space group, $P2_1$, under the same conditions as the complex of human ACE2 and hTor02 RBD. Each of the three structures was determined by molecular replacement using the structure of human ACE2 complexed with hTor02 RBD as the search model (Fig. 1C and D). In each structure, there are two copies of complexes per asymmetric unit; noncrystallographic symmetry averaging between them facilitated structural analysis. The structure of chimeric ACE2 in complex with hTor02 RBD was refined at 2.8 Å to R_{free} of 27.9% (R_{work} of 21.4%), the structure of chimeric ACE2 in complex with cSz02 RBD was refined at 3.1 Å to R_{free} of 30.2% (R_{work} of 22.0%), and the structure of chimeric ACE2 in complex with cGd05 RBD was refined at 2.9 Å to R_{free} of 27.9% (R_{work} of 22.4%) (Table 1). Each of the final models contains residues 19 to 615 of chimeric ACE2 and residues 323 to 502 (except for a disordered loop connecting residues 376 to 381) of RBD. The three complexes share nearly identical overall structures with the complex of human ACE2 and hTor02 RBD, except that the angles between the two lobes of the ACE2 peptidase domain vary slightly, due to flexibility of the hinge region. In particular, despite of the mutations, the N-terminal helix of the chimeric ACE2 in each of the three complexes does not shift or tilt. However, there are important differences in structural details at the interface surrounding RBD residues 479 and 487, revealing the major species barriers between civets and humans for SARS-CoV infections.

Structural basis for host adaptations of residue 479 on SARS-CoV RBD. Residue 479 on SARS-CoV RBD has intricate structural relationships with residues 31 and 35 on host ACE2. In the structure of unbound human ACE2 (28), Lys31 projects into solution (Fig. 3A). In the structure of human ACE2 complexed with hTor02 RBD (11), the side chain of Lys31 folds back, driven by the hydrophobic sheath formed by RBD, and forms a salt bridge with Glu35 of ACE2 (Fig. 3B). In the structure of chimeric ACE2 complexed with hTor02 RBD, residue 31 is a threonine, which cannot form a salt bridge with Glu35 of ACE2; Asn479 of RBD forms hydrophobic interactions with RBD Tyr440 and Tyr442 (Fig. 3C). In the structure of chimeric ACE2 complexed with cSz02 RBD, residue 479 on RBD becomes a lysine whose side chain forms a salt bridge with Glu35 of ACE2, while maintaining hydrophobic interactions with RBD tyrosines (Fig. 3D). In the structure of chimeric ACE2 complexed with cGd05 RBD, residue 479 on RBD becomes an arginine whose side chain forms a bifurcated

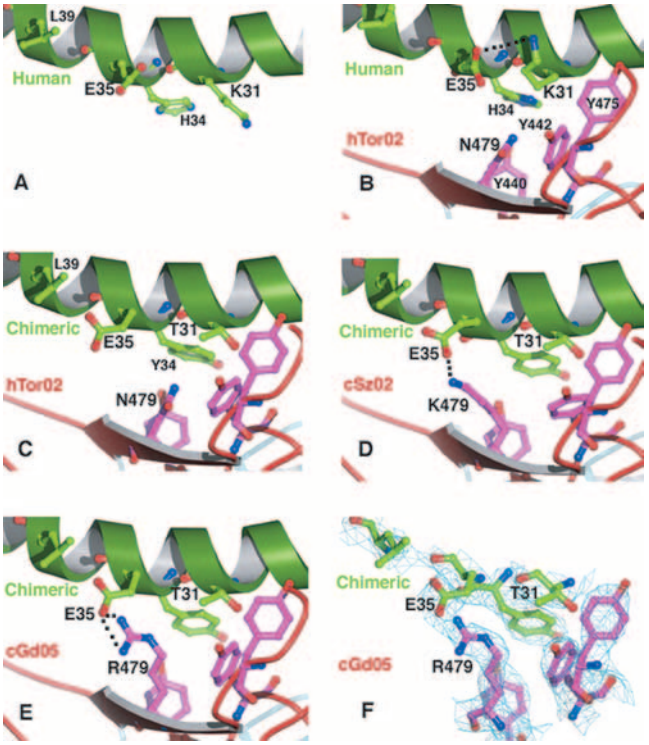

FIG. 3. Structural basis for host adaptations of residue 479 on SARS-CoV RBD. (A) On the surface of unbound human ACE2 (28), Lys31 points into solution. (B) At the interface of human ACE2 and hTor02 (11), Lys31 on ACE2 folds back and forms a salt bridge with Glu35 on ACE2. Asn479 on RBD forms hydrophobic interactions with Tyr440 and Tyr442 on RBD. (C) At the interface of chimeric ACE2 and hTor02, Thr31 cannot form a salt bridge with Glu35 on civet ACE2. Consequently, Glu35 on civet ACE2 is unneutralized. (D) At the interface of chimeric ACE2 and cSz02, Lys479 on RBD forms a salt bridge with Glu35 on civet ACE2 and hydrophobic interactions with tyrosines. (E) At the interface of chimeric ACE2 and cGd05, Arg479 on RBD forms a strong bifurcated salt bridge with Glu35 on civet ACE2 and strong hydrophobic interactions with tyrosines. (F) Electron density map of the interface of chimeric ACE2 and cGd05, as part of a composite-omit map calculated from the refined model of chimeric ACE2 complexed with cGd05 RBD. The illustrations were made using Povscript (4).

salt bridge with Glu35 of ACE2, while maintaining hydrophobic interactions with RBD tyrosines (Fig. 3E and F).

A major species barrier between humans and civets for SARS-CoV infections is the adaptation of residue 479 on RBD to residues 31 and 35 on human ACE2. At the interface of human ACE2 and SARS-CoV, because of the binding of SARS-CoV, Lys31 and Glu35 on ACE2 are forced to form a salt bridge and neutralize each other's charge. At this interface, Lys479 or Arg479 on RBD would be unable to find a salt bridge partner, leaving a free positive charge in a hydrophobic environment and destabilizing the interface. This explains why civet viral isolates with Lys479 or Arg479 on RBD have poor affinities for human ACE2 and consequently cannot infect human cells efficiently and why a single N479K or N479R mutation on human viral RBD decreases the protein's affinity for human ACE2 by over 30-fold (15, 24). At the interface of civet ACE2 and SARS-CoV, there is no salt bridge formed between Thr31 and Glu35 on ACE2, making Glu35 available to form a salt bridge with Lys479 or Arg479 on RBD. As a result, viral isolates with Lys479 or Arg479 on RBD can have high affinities for civet ACE2 and thus can infect civet cells as effectively as those with Asn479 on RBD (15, 24). Therefore, Asn479 on RBD is well adapted to human ACE2 and hence is critical for SARS-CoV to infect humans; Asn479, Lys479, and Arg479 on RBD are all adapted to civet ACE2. In other words, human ACE2 accommodates only a small and uncharged RBD residue at position 479, while civet ACE2 is insensitive to the size and charge of this residue (Table 2).

Structural basis for host adaptations of residue 487 on SARS-CoV RBD. Residue 487 on SARS-CoV RBD is also placed in a complicated structural network at the virus/receptor interface. Like Lys31, in the structure of unbound human ACE2 (28), Lys353 projects into solution (Fig. 4A). In the structure of human ACE2 complexed with hTor02 RBD (11), the side chain of ACE2 Lys353 folds back and is embedded in a hydrophobic tunnel surrounded by Tyr484, Tyr491, and Thr487 on RBD and Tyr41 on ACE2 (Fig. 4B). At the opening of the tunnel is Asp38 on ACE2, which neutralizes the charge of Lys353 and stabilizes the interface. However, the side chain of Asp38 by itself appears not long enough to form a strong and stable salt bridge bond with Lys353, which appears to require support from the γ-methyl group of RBD Thr487. On civet ACE2, residue 38 is a glutamate that has a longer side chain. Consequently, in the structure of chimeric ACE2 complexed with hTor02 RBD, Glu38 and Lys353 on ACE2 form a strong and stable bifurcated salt bridge (Fig. 4C). Similarly, in the structure of chimeric ACE2 complexed with cGd05 RBD or cSz02 RBD, whose residue 487 is a serine instead of a threonine, Glu38 and Lys353 on ACE2 also form a strong and stable bifurcated salt bridge (Fig. 4D and E).

Adaptation of residue 487 on RBD to residues 38 and 353 on human ACE2 appears to be critical in human-human transmission of SARS-CoV. At the interface of human ACE2 and hTor02, the γ-methyl group of the side chain of RBD Thr487 is important for placing the side chain of ACE2 Lys353 in position to form a salt bridge with ACE2 Asp38. Without this methyl group, Lys353 would be unable to form a strong and stable salt bridge with Asp38, leaving a free positive charge in a hydrophobic tunnel (Fig. 4F) and destabilizing the interface. Thus, Thr487 on RBD is critical for the strong binding between human ACE2 and hTor02 RBD and is likely responsible for the severe SARS epidemic in 2002 to 2003. A serine at position 487 on RBD would dramatically decrease the affinity for human ACE2, explaining why a single T487S mutation on human viral RBD decreases the protein's binding affinity for human ACE2 by over 20-fold (15, 24). Hence, Ser487 on hGd03 RBD is likely responsible for the mild symptoms and lack of human-to-human transmission of the sporadic SARS infections in

TABLE 2. Accommodations of SARS-CoV RBD residues by ACE2 residues

ACE2 residue(s)	RBD residue(s)
K31	N479
T31, N31	N479, K479, R479
D38	T487
E38	S487, T487

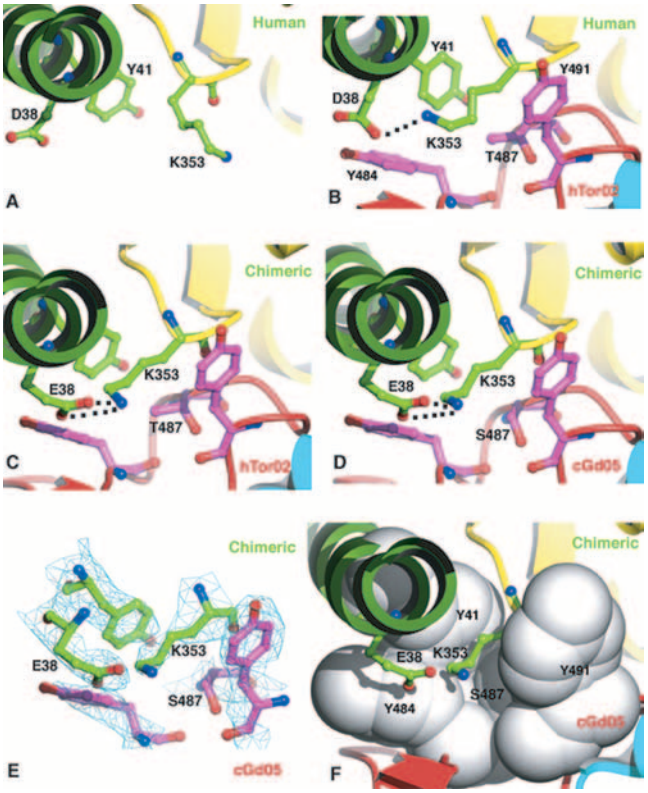

FIG. 4. Structural basis for host adaptations of residue 487 on SARS-CoV RBD. (A) On the surface of unbound human ACE2 (28), Lys353 points into solution. (B) At the interface of human ACE2 and hTor02 (11), Lys353 on ACE2 is embedded in a hydrophobic tunnel surrounded by Thr487 on hTor02 RBD and three tyrosines. Lys353 and Asp38 on ACE2 form a salt bridge, which requires support from RBD Thr487. (C) At the interface of chimeric ACE2 and hTor02, Glu38 and Lys353 on ACE2 form a bifurcated salt bridge, in the presence of RBD Thr487. (D) At the interface of chimeric ACE2 and cGd05, Glu38 and Lys353 on ACE2 form a strong bifurcated salt bridge, in the presence of RBD Ser487. (E) Electron density map of the interface of chimeric ACE2 and cGd05, as part of a composite-omit map calculated from the refined model of chimeric ACE2 complexed with cGd05 RBD. (F) Corey-Pauling-Koltun presentation of the hydrophobic tunnel surrounding ACE2 Lys353 at the interface of chimeric ACE2 and cGd05. The illustrations were made using Povscript (4).

2003 to 2004. On civet ACE2, Lys353 and Glu38 form a tight bifurcated salt bridge, independent of the presence of the γ-methyl group on RBD residue 487. As a result, viral isolates with Ser487 on RBD can have high affinities for civet ACE2 and thus can infect civet cells efficiently (15, 24). Therefore, Thr487 on RBD is well adapted to human ACE2 and appears to be critical for sustained transmission of SARS-CoV in humans; Ser487 and Thr487 on RBD are both adapted to civet ACE2. In other words, human ACE2 only accommodates RBD Thr487, while civets ACE2 has no apparent preference for RBD Thr487 or Ser487 (Table 2).

DISCUSSION

Principles that govern host adaptations and cross-species infections of SARS-CoV. The structural analysis of interfaces between SARS-CoV RBD and host receptors presented above has revealed important principles that govern host adaptations and cross-species infections of SARS-CoV. To effectively infect humans, SARS-CoV needs to undergo two major adaptation mutations at residues 479 and 487 on RBD. The former largely determines whether SARS-CoV can infect humans, whereas the latter likely determines whether SARS-CoV can maintain sustained infections in humans (14, 15). A common theme runs through these two mutations: a free charge embedded in a hydrophobic environment is energetically detrimental to virus/receptor binding. On the other hand, once formed, a salt bridge in a hydrophobic environment is highly stabilizing, due to the low dielectric constant of the hydrophobic environment. Consequently, such free charges must be either neutralized or removed from the interface before effective viral infections can occur. The principles that govern host adaptations and cross-species infections of SARS-CoV may apply to other emerging animal viruses.

Major species barriers between humans and civets for SARS-CoV infections. This study has revealed the structural basis for the major species barriers between humans and civets for SARS-CoV infections. To facilitate structural studies, a chimeric ACE2 bearing the N-terminal helix from civet and the remaining peptidase domain from human was constructed. Solution RBD binding assays showed that like civet ACE2, the chimeric ACE2 binds both civet and human viral RBDs, whereas human ACE2 binds only human viral RBD. Hence, the chimeric ACE2 has the same receptor activity as civet ACE2, and such receptor activity resides mainly on the critical N-terminal helix of the receptor. By determining three crystal structures of the chimeric ACE2 complexed with different civet and human viral RBDs, this study has further characterized four residues on ACE2, three on the N-terminal helix (residues 31, 35, and 38) and a conserved Lys353 outside the helix, as major determinants of the receptor activity of ACE2 (Fig. 5). The interactions of these four residues on ACE2 and two residues, 479 and 487, on SARS-CoV RBD determine the major species barriers between humans and civets for SARS-CoV infections.

Interactions between SARS-CoV and ACE2 from other hosts. Besides humans and civets, SARS-CoV infections have been observed in many other animals, including raccoons, domestic cats, ferrets, and monkeys (14, 26). Interactions between SARS-CoV and ACE2 from these other hosts impose an important initial selection on SARS-CoV infections, whereas other host cell factors may impose selections on later steps of the infections. Sequence alignments of 10 host ACE2s show that among the four ACE2 residues that are critical for civet-human transmission of SARS-CoV, Glu35 is conserved in all of them, whereas residues 31, 38, and 353 have variations (Fig. 5). Residue 353 is a histidine in mouse and rat ACE2s but is a lysine in the other eight ACE2s. His353 does not fit into the virus-receptor interface as well as Lys353 does, and hence mice and rats are poor hosts for any SARS-CoV strain. Among the other eight ACE2s, human, cattle, orangutan, and monkey ACE2s (with residues Lys31 and Asp38) appear to accommodate human viral strain hTor02 (with RBD residues Asn479 and Thr487) but not civet strain cSz02 (Lys479 and Ser487), civet strain cGd05 (Arg479 and Ser487), or human strain hGd03 (Asn479 and Ser487) (Table 2). On the other hand, cat

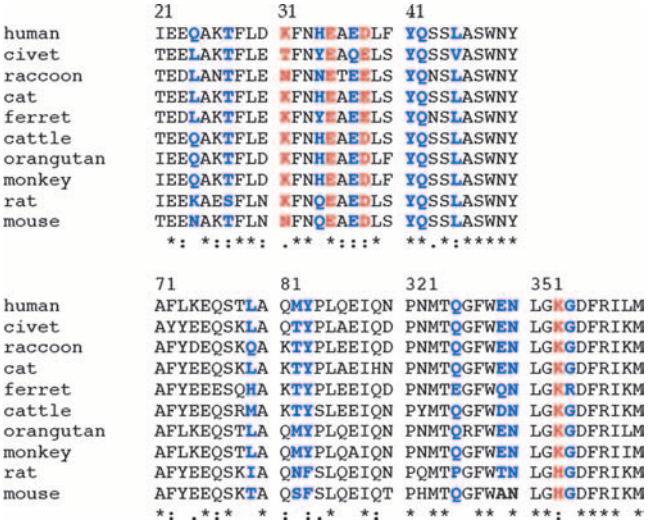

FIG. 5. Sequence alignment of SARS-CoV binding regions of ACE2s from 10 mammals. The GenBank accession numbers are AY623811 (human), AY881174 (civet), AB211998 (raccoon), NM_001039456 (cat), AB 208708 (ferret), NM_001024502 (cattle), Q5RFN1 (orangutan), AY 996037 (monkey), AY881244 (rat), and EF408740 (mouse). The alignment was generated by the ClusterW program. In red are residues that are critical to the major species barriers between hosts for SARS-CoV infections. In blue are residues that directly contact SARS-CoV. Asterisks indicate positions which have a single, fully conserved residue. Colons indicate positions which have strongly conserved residues. Periods indicate positions which have weakly conserved residues.

and ferret ACE2s (with residues Lys31 and Glu38) appear to accommodate both human strains hTor02 and hGd03, whereas civet and raccoon ACE2s (with residues Thr31/Asn31 and Glu38) appear to accommodate all four human and civet viral strains. Therefore, civets and raccoons have the widest range of accommodations for different SARS-CoV strains and thus may play the most important roles in transmission of different SARS-CoV strains. The above analysis provides an important initial evaluation of the interactions between SARS-CoV and ACE2 from hosts other than humans and civets. A complete understanding of these virus-receptor interactions awaits future biochemical and structural studies.

ACKNOWLEDGMENTS

I thank Stephen C. Harrison for his intellectual generosity, Michael Farzan for comments, and staff at APS beamline 19BM for assistance.

This work was supported in part by Minnesota Medical Foundation Research and Equipment grants (to Fang Li), by NIH grant CA-13202 (to Stephen C. Harrison), and by a Minnesota Partnership for Biotechnology and Medical Genomics grant (to the University of Minnesota). Computer resources were provided by the Basic Sciences Computing Laboratory of the University of Minnesota Supercomputing Institute.

REFERENCES

1. **Babcock, G. J., D. J. Esshaki, W. D. Thomas, and D. M. Ambrosino.** 2004. Amino acids 270 to 510 of the severe acute respiratory syndrome coronavirus spike protein are required for interaction with receptor. J. Virol. **78:**4552–4560.
2. **Brunger, A. T., P. D. Adams, G. M. Clore, W. L. DeLano, P. Gros, R. W. Grosse-Kunstleve, J. S. Jiang, J. Kuszewski, M. Nilges, N. S. Pannu, R. J. Read, L. M. Rice, T. Simonson, and G. L. Warren.** 1998. Crystallography & NMR system: a new software suite for macromolecular structure determination. Acta Crystallogr. D **54:**905–921.
3. **Cowtan, K.** 1994. Joint CCP4 and ESF-EACBM Newsl. Protein Crystallogr. **31:**34–38.
4. **Fenn, T. D., D. Ringe, and G. A. Petsko.** 2003. POVScript+: a program for model and data visualization using persistence of vision ray-tracing. J. Appl. Crystallogr. **36:**944–947.
5. **Guan, Y., B. J. Zheng, Y. Q. He, X. L. Liu, Z. X. Zhuang, C. L. Cheung, S. W. Luo, P. H. Li, L. J. Zhang, Y. J. Guan, K. M. Butt, K. L. Wong, K. W. Chan, W. Lim, K. F. Shortridge, K. Y. Yuen, J. S. M. Peiris, and L. L. M. Poon.** 2003. Isolation and characterization of viruses related to the SARS coronavirus from animals in Southern China. Science **302:**276–278.
6. **Jones, T. A., J. Y. Zou, S. W. Cowan, and M. Kjeldgaard.** 1991. Improved methods for building protein models in electron-density maps and the location of errors in these models. Acta Crystallogr. A **47:**110–119.
7. **Ksiazek, T. G., D. Erdman, C. S. Goldsmith, S. R. Zaki, T. Peret, S. Emery, S. X. Tong, C. Urbani, J. A. Comer, W. Lim, P. E. Rollin, S. F. Dowell, A. E. Ling, C. D. Humphrey, W. J. Shieh, J. Guarner, C. D. Paddock, P. Rota, B. Fields, J. DeRisi, J. Y. Yang, N. Cox, J. M. Hughes, J. W. LeDuc, W. J. Bellini, and L. J. Anderson.** 2003. A novel coronavirus associated with severe acute respiratory syndrome. N. Engl. J. Med. **348:**1953–1966.
8. **Lai, M. M. C., and K. V. Holmes.** 2001. Coronaviridae: the viruses and their replication, p. 1163–1186. *In* D. M. Knipe and P. M. Howley (ed.), Fields virology. Lippincott Williams and Wilkins, Philadelphia, PA.
9. **Lee, N., D. Hui, A. Wu, P. Chan, P. Cameron, G. M. Joynt, A. Ahuja, M. Y. Yung, C. B. Leung, K. F. To, S. F. Lui, C. C. Szeto, S. Chung, and J. J. Y. Sung.** 2003. A major outbreak of severe acute respiratory syndrome in Hong Kong. N. Engl. J. Med. **348:**1986–1994.
10. **Li, F., W. H. Li, M. Farzan, and S. C. Harrison.** 2006. Interactions between SARS coronavirus and its receptor. Adv. Exp. Med. Biol. **581:**229–234.
11. **Li, F., W. H. Li, M. Farzan, and S. C. Harrison.** 2005. Structure of SARS coronavirus spike receptor-binding domain complexed with receptor. Science **309:**1864–1868.
12. **Li, W. H., T. C. Greenough, M. J. Moore, N. Vasilieva, M. Somasundaran, J. L. Sullivan, M. Farzan, and H. Choe.** 2004. Efficient replication of severe acute respiratory syndrome coronavirus in mouse cells is limited by murine angiotensin-converting enzyme 2. J. Virol. **78:**11429–11433.
13. **Li, W. H., M. J. Moore, N. Vasilieva, J. H. Sui, S. K. Wong, M. A. Berne, M. Somasundaran, J. L. Sullivan, K. Luzuriaga, T. C. Greenough, H. Choe, and M. Farzan.** 2003. Angiotensin-converting enzyme 2 is a functional receptor for the SARS coronavirus. Nature **426:**450–454.
14. **Li, W. H., S. K. Wong, F. Li, J. H. Kuhn, I. C. Huang, H. Choe, and M. Farzan.** 2006. Animal origins of the severe acute respiratory syndrome coronavirus: insight from ACE2–S-protein interactions. J. Virol. **80:**4211–4219.
15. **Li, W. H., C. S. Zhang, J. H. Sui, J. H. Kuhn, M. J. Moore, S. W. Luo, S. K. Wong, I. C. Huang, K. M. Xu, N. Vasilieva, A. Murakami, Y. Q. He, W. A. Marasco, Y. Guan, H. Y. Choe, and M. Farzan.** 2005. Receptor and viral determinants of SARS-coronavirus adaptation to human ACE2. EMBO J. **24:**1634–1643.
16. **Liang, G. D., Q. X. Chen, J. G. Xu, Y. F. Liu, W. Lim, J. S. M. Peiris, L. J. Anderson, L. Ruan, H. Li, B. Kan, B. Di, P. Cheng, K. H. Chan, D. D. Erdman, S. Y. Gu, X. G. Yan, W. L. Liang, D. H. Zhou, L. Haynes, S. M. Duan, X. Zhang, H. Zheng, Y. Gao, S. X. Tong, D. X. Li, L. Fang, P. Z. Qin, and W. B. Xu.** 2004. Laboratory diagnosis of four recent sporadic cases of community-acquired SARS, Guangdong Province, China. Emerg. Infect. Dis. **10:**1774–1781.
17. **Liu, L., Q. Fang, F. Deng, H. Z. Wang, C. E. Yi, L. Ba, W. J. Yu, R. D. Lin, T. S. Li, Z. H. Hu, D. D. Ho, L. Q. Zhang, and Z. W. Chen.** 2007. Natural mutations in the receptor binding domain of spike glycoprotein determine the reactivity of cross-neutralization between palm civet coronavirus and severe acute respiratory syndrome coronavirus. J. Virol. **81:**4694–4700.
18. **Marra, M. A., S. J. M. Jones, C. R. Astell, R. A. Holt, A. Brooks-Wilson, Y. S. N. Butterfield, J. Khattra, J. K. Asano, S. A. Barber, S. Y. Chan, A. Cloutier, S. M. Coughlin, D. Freeman, N. Girn, O. L. Griffith, S. R. Leach, M. Mayo, H. McDonald, S. B. Montgomery, P. K. Pandoh, A. S. Petrescu, A. G. Robertson, J. E. Schein, A. Siddiqui, D. E. Smailus, J. E. Stott, G. S. Yang, F. Plummer, A. Andonov, H. Artsob, N. Bastien, K. Bernard, T. F. Booth, D. Bowness, M. Czub, M. Drebot, L. Fernando, R. Flick, M. Garbutt, M. Gray, A. Grolla, S. Jones, H. Feldmann, A. Meyers, A. Kabani, Y. Li, S. Normand, U. Stroher, G. A. Tipples, S. Tyler, R. Vogrig, D. Ward, B. Watson, R. C. Brunham, M. Krajden, M. Petric, D. M. Skowronski, C. Upton, and R. L. Roper.** 2003. The genome sequence of the SARS-associated coronavirus. Science **300:**1399–1404.
19. **McCray, P. B., L. Pewe, C. Wohlford-Lenane, M. Hickey, L. Manzel, L. Shi, J. Netland, H. P. Jia, C. Halabi, C. D. Sigmund, D. K. Meyerholz, P. Kirby, D. C. Look, and S. Perlman.** 2007. Lethal infection of K18-hACE2 mice infected with severe acute respiratory syndrome coronavirus. J. Virol. **81:**813–821.
20. **Moore, M. J., T. Dorfman, W. H. Li, S. K. Wong, Y. H. Li, J. H. Kuhn, J. Coderre, N. Vasilieva, Z. C. Han, T. C. Greenough, M. Farzan, and H. Choe.** 2004. Retroviruses pseudotyped with the severe acute respiratory syndrome coronavirus spike protein efficiently infect cells expressing angiotensin-converting enzyme 2. J. Virol. **78:**10628–10635.
21. **Murshudov, G. N., A. A. Vagin, A. Lebedev, K. S. Wilson, and E. J. Dodson.** 1999. Efficient anisotropic refinement of macromolecular structures using FFT. Acta Crystallogr. D **55:**247–255.

22. **Otwinowski, Z., and W. Minor.** 1997. Processing of X-ray diffraction data collected in oscillation mode. Macromol. Crystallogr. A **276:**307–326.
23. **Peiris, J. S. M., S. T. Lai, L. L. M. Poon, Y. Guan, L. Y. C. Yam, W. Lim, J. Nicholls, W. K. S. Yee, W. W. Yan, M. T. Cheung, V. C. C. Cheng, K. H. Chan, D. N. C. Tsang, R. W. H. Yung, T. K. Ng, and K. Y. Yuen.** 2003. Coronavirus as a possible cause of severe acute respiratory syndrome. Lancet **361:**1319–1325.
24. **Qu, X. X., P. Hao, X. J. Song, S. M. Jiang, Y. X. Liu, P. G. Wang, X. Rao, H. D. Song, S. Y. Wang, Y. Zuo, A. H. Zheng, M. Luo, H. L. Wang, F. Deng, H. Z. Wang, Z. H. Hu, M. X. Ding, G. P. Zhao, and H. K. Deng.** 2005. Identification of two critical amino acid residues of the severe acute respiratory syndrome coronavirus spike protein for its variation in zoonotic tropism transition via a double substitution strategy. J. Biol. Chem. **280:**29588–29595.
25. **Rota, P. A., M. S. Oberste, S. S. Monroe, W. A. Nix, R. Campagnoli, J. P. Icenogle, S. Penaranda, B. Bankamp, K. Maher, M. H. Chen, S. X. Tong, A. Tamin, L. Lowe, M. Frace, J. L. DeRisi, Q. Chen, D. Wang, D. D. Erdman, T. C. T. Peret, C. Burns, T. G. Ksiazek, P. E. Rollin, A. Sanchez, S. Liffick, B. Holloway, J. Limor, K. McCaustland, M. Olsen-Rasmussen, R. Fouchier, S. Gunther, A. Osterhaus, C. Drosten, M. A. Pallansch, L. J. Anderson, and W. J. Bellini.** 2003. Characterization of a novel coronavirus associated with severe acute respiratory syndrome. Science **300:**1394–1399.
26. **Shi, Z. L., and Z. H. Hu.** 2008. A review of studies on animal reservoirs of the SARS coronavirus. Virus Res. **133:**74–87.
27. **Song, H. D., C. C. Tu, G. W. Zhang, S. Y. Wang, K. Zheng, L. C. Lei, Q. X. Chen, Y. W. Gao, H. Q. Zhou, H. Xiang, H. J. Zheng, S. W. W. Chern, F. Cheng, C. M. Pan, H. Xuan, S. J. Chen, H. M. Luo, D. H. Zhou, Y. F. Liu, J. F. He, P. Z. Qin, L. H. Li, Y. Q. Ren, W. J. Liang, Y. D. Yu, L. Anderson, M. Wang, R. H. Xu, X. W. Wu, H. Y. Zheng, J. D. Chen, G. D. Liang, Y. Gao, M. Liao, L. Fang, L. Y. Jiang, H. Li, F. Chen, B. Di, L. J. He, J. Y. Lin, S. X. Tong, X. G. Kong, L. Du, P. Hao, H. Tang, A. Bernini, X. J. Yu, O. Spiga, Z. M. Guo, H. Y. Pan, W. Z. He, J. C. Manuguerra, A. Fontanet, A. Danchin, N. Niccolai, Y. X. Li, C. I. Wu, and G. P. Zhao.** 2005. Cross-host evolution of severe acute respiratory syndrome coronavirus in palm civet and human. Proc. Natl. Acad. Sci. USA **102:**2430–2435.
28. **Towler, P., B. Staker, S. G. Prasad, S. Menon, J. Tang, T. Parsons, D. Ryan, M. Fisher, D. Williams, N. A. Dales, M. A. Patane, and M. W. Pantoliano.** 2004. ACE2 X-ray structures reveal a large hinge-bending motion important for inhibitor binding and catalysis. J. Biol. Chem. **279:**17996–18007.
29. **Wong, S. K., W. H. Li, M. J. Moore, H. Choe, and M. Farzan.** 2004. A 193-amino acid fragment of the SARS coronavirus S protein efficiently binds angiotensin-converting enzyme 2. J. Biol. Chem. **279:**3197–3201.
30. **Wu, D. L., C. C. Tu, C. Xin, H. Xuan, Q. W. Meng, Y. G. Liu, Y. D. Yu, Y. T. Guan, Y. Jiang, X. N. Yin, G. Crameri, M. P. Wang, C. W. Li, S. W. Liu, M. Liao, L. Feng, H. Xiang, J. F. Sun, J. D. Chen, Y. W. Sun, S. L. Gu, N. H. Liu, D. X. Fu, B. T. Eaton, L. F. Wang, and X. G. Kong.** 2005. Civets are equally susceptible to experimental infection by two different severe acute respiratory syndrome coronavirus isolates. J. Virol. **79:**2620–2625.
31. **Xiao, X. D., S. Chakraborti, A. S. Dimitrov, K. Gramatikoff, and D. S. Dimitrov.** 2003. The SARS-CoV S glycoprotein: expression and functional characterization. Biochem. Biophys. Res. Commun. **312:**1159–1164.
32. **Yu, I. T. S., Y. G. Li, T. W. Wong, W. Tam, A. T. Chan, J. H. W. Lee, D. Y. C. Leung, and T. Ho.** 2004. Evidence of airborne transmission of the severe acute respiratory syndrome virus. N. Engl. J. Med. **350:**1731–1739.
33. **Zhong, N. S.** 2004. Management and prevention of SARS in China. Philos. Trans. R. Soc. London B **359:**1115–1116.